HYPERSPECTRAL UNMIXING VIA PLUG-AND-PLAY PRIORS

Xiuheng Wang, Min Zhao, Jie Chen

Center of Intelligent Acoustics and Immersive Communications,
School of Marine Science and Technology, Northwestern Polytechinical University, China
{xiuheng.wang, minzhao}@mail.nwpu.edu.cn, dr.jie.chen@ieee.org

ABSTRACT

Hyperspectral unmixing aims at separating a mixed pixel into a set of pure spectral signatures and their corresponding fractional abundances. Investigating prior spatial and spectral information to regularize the unmixing problem can effectively improve the estimation performance. However, handcrafting a powerful regularizer is a non-trivial task and complex regularizers introduce extra difficulties in solving the optimization problem. In this paper, we present a flexible spectral unmixing method using plug-and-play priors. This method benefits from the alternating direction method of multipliers (ADMM) to decompose the optimization problem into iterative subproblems and incorporates the image denoisers as prior models in a subproblem. In this form, we can plug in various image denoising operations to bypass handcrafting regularizers. We demonstrate the superiority of the proposed unmixing method comparing with other state-of-the-art methods both on synthetic data and real airborne data.

Index Terms— Hyperspectral unmixing, prior modeling, ADMM, plug-and-play, image denoising

1. INTRODUCTION

Hyperspectral imaging is widely used in agricultural monitoring, field surveillance and camouflage tests because it provides 2D images along with rich spectral information. However, hyperspectral pixels are often a mixture of spectra of several pure materials due to the low spatial resolution of imaing devices, the presence of microscopic material and multiple scattering. Hyperspectral unmixing is thus an important technique in hyperspectral data analysis. It decomposes the mixed spectra into a collection of endmembers and abundances associated with each endmember [1, 2].

Considering the spatial and contextual information existing in images, it can be beneficial to use spatial and spectral priors to enhance hyperspectral unmixing performance rather than conduct spectral unmixing on individual pixels. Using extra regularization terms in formulated optimization problems is one efficient way to incorporate these priors. One such regularizer is the total-variation (TV) regularizer, which has been widely used in image processing [3, 4]. This regularizer aims to promote the piecewise spatial consistency of estimated abundances. Graph regularization is another general method to encode the spatial and spectral similarity for unmixing [5, 6]. The work [7] uses nonlocal smoothness to exploit the similar structures in abundance results. In [8, 9], markov random field (MRF) is used to take into account the possible spatial correlations between the pixels and obtain the priors about spatial homogeneous regions before unmixing. The works [10, 11] use image segmentation method, such as superpixel, to generate the spatial groups and get local pixels with homogeneous spectra.

Considering the inherent spatial-spectral information exists in hyperspectral images, it is important to define proper priors to enhance the unmixing performance. However, it is not trivial to handcraft a good regularizer, and complex regularizers may increase the difficulty of solving the optimization problem. Recently, benefitting form the variable splitting techniques, many plug-and-play methods have been proposed to solve various hyperspectral image inverse problems [12–14]. In our work, we aim to use priors of reconstructed images to constrain the solution and propose a flexible hyperspectral unmixing method using plug-and-play priors. Based on the ADMM [15], our approach plugs denoisers as a module into an iterative algorithm to solve the unmixing problem, which allows various image denoisers (linear or nonlinear, band-wise or 3D) to replace the design of regularizers. To the best of our knowledge, this is the first time applying the plug-and-play priors in hyperspectral unmixing. Experimental results show the effectiveness of the proposed strategy.

2. PROBLEM FORMULATION

Consider a hyperspectral image $Y_{3\mathrm{D}} \in \mathbb{R}^{B\times L\times W}$ with the number of spectral dimensions B, the size of rows and columns in the image L and W. We reshape the 3D hyperspectral image cube into 2D matrix $\mathbf{Y} \in \mathbb{R}^{B\times N}$ where

X. Wang and M. Zhao contributed equally to this work. The work of J. Chen was funded in part by National Key Research and Development Program of China under grant 2018AAA0102200, NSFC under grants 61671382, and in part by 111 project (B18041). Corresponding author: J. Chen.

$N = L \times W$ is the total number of hyperspectral pixels. Considering the linear unmixing model, each pixel in the image is a linear mixture of endmember spectra weighted by the corresponding fractional abundances. Then the hyperspectral pixel $\mathbf{y}_i \in \mathbb{R}^B$ can be formulated as:

$$\mathbf{y}_i = \mathbf{E}\mathbf{a}_i + \mathbf{n}_i \tag{1}$$

where $\mathbf{E} = [\mathbf{e}_1, \mathbf{e}_2, \cdots, \mathbf{e}_R] \in \mathbb{R}^{B\times R}$ is a matrix containing R spectral signatures of the endmembers, $\mathbf{a}_i \in \mathbb{R}^R$ is the corresponding abundance vector, $\mathbf{n}_i \in \mathbb{R}^B$ is the additive independent and identically distributed Gaussian noise. The abundances refer to the fraction of certain endmember present at a pixel. They are enforced to satisfy two physical constraints: abundance nonnegative constraint (ANC) and abundance sum-to-one constraint (ASC):

$$\mathbf{a}_i \geq \mathbf{0}, \quad \text{for } i = 1, \cdots, N, \tag{2}$$

$$\mathbf{1}^T\mathbf{a}_i = 1, \quad \text{for } i = 1, \cdots, N \tag{3}$$

where $\mathbf{1} \in \mathbb{R}^B$ represents all-one vector. We estimate the abundances with the given endmember matrix $\mathbf{E}$ and it leads to solve the following problem:

$$\begin{aligned} \hat{\mathbf{A}} &= \arg\min_{\mathbf{A}} \sum_{i=1}^{N} \|\mathbf{y}_i - \mathbf{E}\mathbf{a}_i\|^2 \\ &\text{s.t.} \quad \mathbf{a}_i \geq \mathbf{0}, \quad \mathbf{1}^T\mathbf{a}_i = 1, \quad \text{for } i = 1, \cdots, N \end{aligned} \tag{4}$$

where $\mathbf{A} = [\mathbf{a}_1, \mathbf{a}_2, \cdots, \mathbf{a}_N] \in \mathbb{R}^{R\times N}$ denotes the abundance matrix. Considering inherent spatial-spectral duality exists in reconstructed hyperspectral images, a significant amount of regularizers have been added in the object function to improve the unmixing performance. Then the objective function (4) can be formulated as:

$$\begin{aligned} \hat{\mathbf{A}} &= \arg\min_{\mathbf{A}} \sum_{i=1}^{N} \|\mathbf{y}_i - \mathbf{E}\mathbf{a}_i\|^2 + \lambda\, \Phi(\mathbf{E}\mathbf{A}) \\ &\text{s.t.} \quad \mathbf{a}_i \geq \mathbf{0}, \quad \mathbf{1}^T\mathbf{a}_i = 1, \quad \text{for } i = 1, \cdots, N \end{aligned} \tag{5}$$

where the first squared-error term is called data fidelity term, $\Phi(\mathbf{E}\mathbf{A})$ is the regularizer defined to further promote the desired property, and λ is the positive parameter controlling the relative weight of each term. In hyperspectral unmixing, the priors of images are often encoded in $\Phi(\mathbf{E}\mathbf{A})$.

3. PROPOSED METHOD

Instead of using a handcrafted regularizer $\Phi(\mathbf{E}\mathbf{A})$, we propose to directly use priors from reconstructed hyperspectral data and incorporate it into model-based optimization to tackle the regularized unmixing problem. In our work, we utilize the variable splitting technique ADMM to solve the equation (5) for its competitive convergence properties. More specifically, we transform problem (5) into two subproblems, namely, a quadratic programming (QP) problem and a image denoising problem. These subproblems are iteratively solved until the convergence criterion is met.

By introducing an auxiliary variable $\mathbf{Z}$, the optimization problem (5) can be written in the equivalent form:

$$\begin{aligned} \hat{\mathbf{A}} &= \arg\min_{\mathbf{A}} \sum_{i=1}^{N} \frac{1}{2}\|\mathbf{y}_i - \mathbf{E}\mathbf{a}_i\|^2 + \lambda\Phi(\mathbf{Z}) \\ &\text{s.t.} \quad \mathbf{Z} = \mathbf{E}\mathbf{A} \\ &\qquad \mathbf{a}_i \geq \mathbf{0}, \quad \mathbf{1}^T\mathbf{a}_i = 1, \quad \text{for } i = 1, \cdots, N. \end{aligned} \tag{6}$$

The associated augmented Lagrangian function for this problem is given by:

$$\begin{aligned} \mathcal{L}_\rho(\mathbf{A}, \mathbf{Z}, \mathbf{V}) = \arg\min_{\mathbf{A}} &\sum_{i=1}^{N} \frac{1}{2}\|\mathbf{y}_i - \mathbf{E}\mathbf{a}_i\|^2 + \lambda\Phi(\mathbf{Z}) \\ &+ \mathbf{V}^T(\mathbf{E}\mathbf{A} - \mathbf{Z}) + \frac{\rho}{2}\|\mathbf{E}\mathbf{A} - \mathbf{Z}\|_F^2 \\ \text{s.t.} \quad &\mathbf{a}_i \geq \mathbf{0}, \ \mathbf{1}^T\mathbf{a}_i = 1, \ \text{for } i = 1, \cdots, N \end{aligned} \tag{7}$$

where $\mathbf{V}$ is the dual variable, $\|\cdot\|_F$ is the Frobenius-norm of the matrix, and $\rho > 0$ is the penalty parameter. By scaling $\mathbf{V}$ as $\mathbf{U} = \frac{1}{\rho}\mathbf{V}$, (7) can be solved by repeating the following steps until convergence:

$$\begin{aligned} \mathbf{A}_{k+1} = \arg\min_{\mathbf{A}} &\sum_{i=1}^{N} \frac{1}{2}\|\mathbf{y}_i - \mathbf{E}\mathbf{a}_i\|^2 + \frac{\rho_k}{2}\|\mathbf{E}\mathbf{A} - \tilde{\mathbf{X}}_k\|_F^2 \\ \text{s.t.} \quad &\mathbf{a}_i \geq \mathbf{0}, \quad \mathbf{1}^T\mathbf{a}_i = 1, \quad \text{for } i = 1, \cdots, N. \end{aligned} \tag{8}$$

$$\mathbf{Z}_{k+1} = \arg\min_{\mathbf{Z}} \lambda\Phi(\mathbf{Z}) + \frac{\rho_k}{2}\|\tilde{\mathbf{Z}}_k - \mathbf{Z}\|_F^2 \tag{9}$$

$$\mathbf{U}_{k+1} = \mathbf{U}_k + \mathbf{E}\mathbf{A}_{k+1} - \mathbf{Z}_{k+1} \tag{10}$$

$$\rho_{k+1} = \alpha\rho_k \tag{11}$$

where $\tilde{\mathbf{X}}_k = \mathbf{Z}_k - \mathbf{U}_k$ and $\tilde{\mathbf{Z}}_k = \mathbf{E}\mathbf{A}_{k+1} + \mathbf{U}_k$. In order to comply with the constraint $\mathbf{Z} = \mathbf{E}\mathbf{A}$, we tighten the penalty function $\|\mathbf{E}\mathbf{A} - \mathbf{Z}\|_F^2$ by updating ρ in (11) where α is the scaling factor. The subproblem (8) is an inversion operator and solving $\mathbf{a}_{k+1,i}$ is a QP problem which can be reformulated as

$$\begin{aligned} \mathbf{a}_{k+1,i} &= \arg\min_{\mathbf{a}_i} \frac{1}{2}\|\mathbf{y}_i - \mathbf{E}\mathbf{a}_i\|^2 + \frac{\rho_k}{2}\|\mathbf{E}\mathbf{a}_i - \tilde{\mathbf{x}}_{k,i}\|^2 \\ &= \arg\min_{\mathbf{a}_i} \frac{1}{2}\mathbf{a}_i^T\mathbf{H}\mathbf{a}_i + \mathbf{f}^T\mathbf{a}_i \\ &\quad \text{s.t.} \quad \mathbf{a}_i \geq \mathbf{0}, \quad \mathbf{1}^T\mathbf{a}_i = 1. \end{aligned} \tag{12}$$

where $\mathbf{H} = \mathbf{E}^T\mathbf{E}$ and $\mathbf{f} = -\frac{1}{\rho_k+1}\mathbf{E}^T(\mathbf{y}_i + \rho_k\tilde{\mathbf{x}}_{k,i})$. The QP problem in (12), a standard fully constrained least squares (FCLS) form, can be solved by a generic QP solver. The subproblem involving regularizer term in (9) can be rewritten as

$$\mathbf{Z}_{k+1} = \arg\min_{\mathbf{Z}} \frac{1}{2(\sqrt{\lambda/\rho_k})^2}\|\tilde{\mathbf{Z}}_k - \mathbf{Z}\|_F^2 + \Phi(\mathbf{Z}). \tag{13}$$

Table 1. Abundance RMSE comparison of the synthetic data. "Pro-NLM" represents the proposed method with the NLM denoiser, 'Pro-BM3D" represents the proposed method with the BM3D denoiser, and 'Pro-BM4D" represents the proposed method with the BM4D denoiser.

	FCLS	SUnSAL	SUnSAL-TV	CSUnL0	SCHU	Pro-NLM	Pro-BM3D	Pro-BM4D
5 dB	0.0897	0.1078	0.1074	0.1078	0.1078	**0.0866**	0.0890	0.0882
10 dB	0.0581	0.0695	0.0673	0.0696	0.0696	0.0552	0.0566	**0.0550**
20 dB	0.0200	0.0243	0.0222	0.0242	0.0242	0.0189	0.0187	**0.0172**
30 dB	0.0064	0.0077	0.0067	0.0077	0.0268	**0.0062**	0.0063	0.0064

Boldface numbers denote the lowest RMSEs and underlined numbers denote the second lowest RMSEs.

Algorithm 1 Plug-and-play priors framework for hyperspectral unmixing.

Input: Hyperspectral image $\mathbf{Y}$, endmembers $\mathbf{E}$, number of hyperspectral pixels N, regularization parameter λ, penalty factor ρ, number of iterations K, scaling factor α.
Output: Fractional abundance $\mathbf{A}$.
Initialize $\mathbf{A} = \mathbf{A}_0$, auxiliary variable $\mathbf{Z}_0 = \mathbf{E}\mathbf{A}_0$, scaled dual variable $\mathbf{U}_0 = \mathbf{0}$, $k = 0$.
while Stopping criteria are not met and $k \leq K$ **do**
  $\tilde{\mathbf{X}}_k = \mathbf{Z}_k - \mathbf{U}_k$
  for $i = 1$ to N **do**
    Calculate $\mathbf{a}_{k+1,i}$ by using a generic QP solver
  end for
  $\tilde{\mathbf{Z}}_k = \mathbf{E}\mathbf{A}_{k+1} + \mathbf{U}_k$
  $\mathbf{Z}_{k+1} = \mathit{Denoiser}(\mathcal{T}(\tilde{\mathbf{Z}}_k), \sqrt{\lambda/\rho_k})$
  $\mathbf{U}_{k+1} = \mathbf{U}_k + \mathbf{E}\mathbf{A}_{k+1} - \mathbf{Z}_{k+1}$
  $\rho_{k+1} = \alpha\rho_k$
  $k = k + 1$
end while

According to Bayesian theory, (13) is corresponding to obtain the clean hyperspectral image $\mathbf{Z}_{k+1}$ by a Gaussian denoiser to remove noise with level $\sqrt{\lambda/\rho_k}$ from the noisy observation $\tilde{\mathbf{Z}}_k$. In other words, we can "plug in" denoising operators that can be used for the regularization term. We rewrite (13) as follows:

$$\mathbf{Z}_{k+1} = \mathit{Denoiser}(\mathcal{T}(\tilde{\mathbf{Z}}_k), \sqrt{\lambda/\rho_k}) \tag{14}$$

where $\mathcal{T}(\cdot)$ is an operator to reshape 2D matrix to 3D data cube. In this way, the denoiser can fully use the spatial and spectral information of the hyperspectral image. Then the hyperspectral image priors encoded in $\Phi(\mathbf{E}\mathbf{A})$ is replaced by the denoising operator (14), which is so-called plug-and-play priors.

With the various choices of image denoisers, the plug-and-play priors unmixing framework is flexible. The whole procedure of our scheme is summarized in Algorithm 1.

4. EXPERIMENTS

In this section, experiments were conducted to show the effectiveness of the proposed method. Three typical denoising techniques were used for the plug-and-play priors framework, namely, the linear denoiser NLM [16] as 2D band-wise approaches; the nonlinear denoiser BM3D [17] as 2D band-wise approaches; the nonlinear denoiser BM4D [18] as the 3D cube-based approache extended from the 2D.

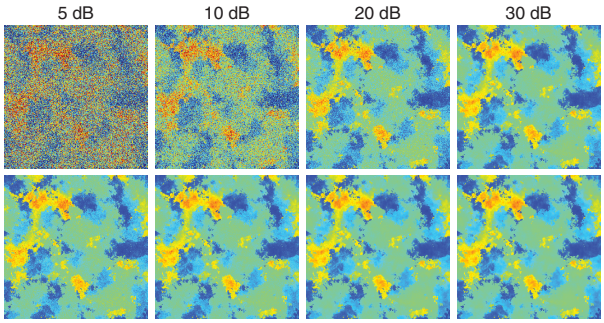

Fig. 1. Comparison between original images (first row) and reconstructed images (second row) at the 190th band.

In the experiments, parameter λ was set to 0.0001, ρ was set to 0.0004 and α was set to 1.2, expect for denoiser BM4D with $\lambda = 0.0005$ and $\rho = 0.004$. The number of iterations K in Algorithm 1 was set to 18, which was sufficient to ensure the convergence. Several unmixing algorithms with handcrafted regularizers were conducted to compare the performance, including:

- **The FCLS method [19]:** This classical linear unmixing method that solves the least-square problem subject to ANC and ASC, without using other priors.
- **SUnSAL [20]**: This algorithm is a sparse unmixing method using the variable splitting and augmented Lagrangian method.
- **SUnSAL-TV [3]**: This method introduces the total-variation norm into the SUnSAL method for providing a spatial regularization.
- **CSUnL0 [21]:** This is a collaborative sparse spectral unmixing method using ℓ_0 norm.
- **SCHU [11]:** This method uses a superpixel based constructing process and graph-based regularization for hyperspectral unmixing.

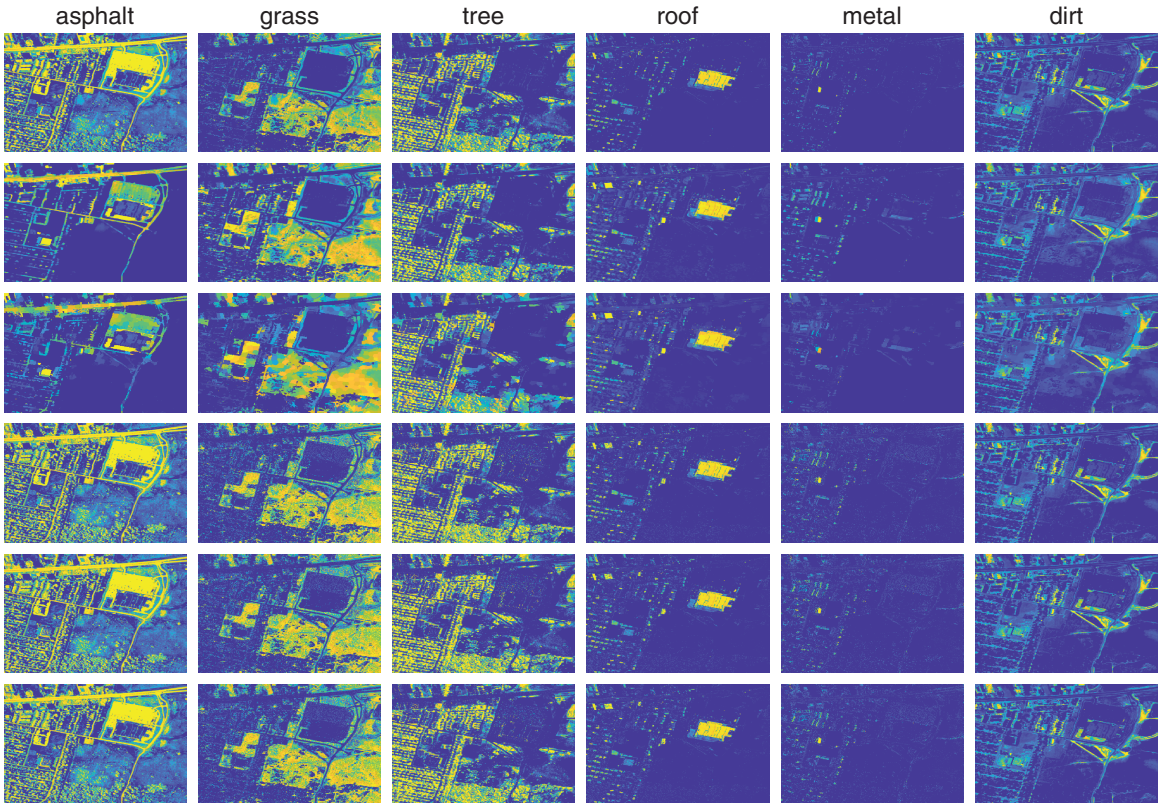

Fig. 2. Estimated abundance maps. From top to bottom: FCLS, SUnSAL-TV, SCHU, Pro-NLM, Pro-BM3D, Pro-BM4D.

4.1. Synthetic data

This dataset was generated using four pure spectral signatures which were selected from USGS digital spectral library as endmembers ($R = 4$). Abundances were generated using HYDRA toolbox. The spatial resolution of this dataset was set to 256×256, and the spectra consists of 224 bands. Gaussian noise with four SNR levels (5 dB, 10 dB, 20 dB and 30 dB) were added to the linearly mixed data. The performance of abundance estimation was evaluated by the root mean square error (RMSE), calculated as follows:

$$\text{RMSE} = \sqrt{\frac{1}{NR}\sum_{i=1}^{N}\left\|\mathbf{a}_i - \hat{\mathbf{a}}_i\right\|^2} \qquad (15)$$

where N represents the number of pixels, $\mathbf{a}_i$ and $\hat{\mathbf{a}}_i$ denote the true and estimated abundance vectors of the ith pixel. The RMSE results are reported in Table 1. From these results we can see that the proposed unmixing scheme using plug-and-play priors unmixing method shows the best results in many cases. In order to better illustrate the effect of the plug-and-play priors, the 190th band of the noisy data and the reconstructed data from Pro-NLM under four SNRs are shown in Fig.1. It is clear that using learnt priors enabled to capture latent structures of the data and significantly enhanced the reconstructed image.

4.2. Real data

The proposed unmixing method was then evaluated by the widely used real unmixing dataset Urban. This dataset consists of 210 spectral bands, and the bands affected by water vapor and atmosphere are removed with 162 bands remained. The spatial size of this data is 307×307. Urban data contains 6 pure materials, including "asphalt", "grass", "tree", "roof", "metal", and "dirt". VCA algorithm [22] was used to extract these endmembers. Our results were compared with all the state-of-the-art algorithms considered previously. Fig. 2 shows the estimated abundance maps. We observe that our proposed method provides a clearer and sharper results.

5. CONCLUSION

In this paper, we proposed to conduct the hyperspectral unmixing with plug-and-play priors, which provided a flexible framework by using various image denoisers in the unmixing process. Specially, learnt priors enabled to capture inherent image structures and allowed enhanced performance. In the experiments, several denoisers were plugged into the ADMM to replace defining prior information. Both synthetic and real data experiment results demonstrated that the of our proposed strategy outperformed the state-of-the-art unmixing algorithms.

6. REFERENCES

[1] R. Heylen, M. Parente, and P. Gader, "A review of nonlinear hyperspectral unmixing methods," *IEEE J. Sel. Top. Appl. Earth Observat. Remote Sens.*, vol. 7, no. 6, pp. 1844–1868, 2014.

[2] J. Bioucas-Dias, A. Plaza, N. Dobigeon, M. Parente, Q. Du, P. Gader, and J. Chanussot, "Hyperspectral unmixing overview: Geometrical, statistical, and sparse regression-based approaches," *IEEE J. Sel. Top. Appl. Earth Observat. Remote Sens.*, vol. 5, no. 2, pp. 354–379, 2012.

[3] M. Iordache, J. Bioucas-Dias, and A. Plaza, "Total variation spatial regularization for sparse hyperspectral unmixing," *IEEE Trans. Geosci. Remote Sens.*, vol. 50, no. 11, pp. 4484–4502, 2012.

[4] W. He, H. Zhang, and L. Zhang, "Total variation regularized reweighted sparse nonnegative matrix factorization for hyperspectral unmixing," *IEEE Trans. Geosci. Remote Sens.*, vol. 55, no. 7, pp. 3909–3921, 2017.

[5] R. Ammanouil, A. Ferrari, and C. Richard, "A graph laplacian regularization for hyperspectral data unmixing," in *Proc. of IEEE International Conference on Acoustics, Speech and Signal Processing (ICASSP)*, 2015, pp. 1637–1641.

[6] Z. Li, J. Chen, and S. Rahardja, *Hyperspectral Imaging in Agriculture, Food and Environment*, chapter Graph construction for hyperspectral data unmixing, IntechOpen, 2018.

[7] Y. Zhong, R. Feng, and L. Zhang, "Non-local sparse unmixing for hyperspectral remote sensing imagery," *IEEE J. Sel. Top. Appl. Earth Observat. Remote Sens.*, vol. 7, no. 6, pp. 1889–1909, 2013.

[8] O. Eches, N. Dobigeon, and J. Tourneret, "Enhancing hyperspectral image unmixing with spatial correlations," *IEEE Trans. Geosci. Remote Sens.*, vol. 49, no. 11, pp. 4239–4247, 2011.

[9] O. Eches, J. Benediktsson, N. Dobigeon, and J. Tourneret, "Adaptive markov random fields for joint unmixing and segmentation of hyperspectral images," *IEEE Trans. Image Process.*, vol. 22, no. 1, pp. 5–16, 2012.

[10] X. Wang, Y. Zhong, L. Zhang, and Y. Xu, "Spatial group sparsity regularized nonnegative matrix factorization for hyperspectral unmixing," *IEEE Trans. Geosci. Remote Sens.*, vol. 55, no. 11, pp. 6287–6304, 2017.

[11] Z. Li, J. Chen, and S. Rahardja, "Superpixel construction for hyperspectral unmixing," in *2018 26th European Signal Processing Conference (EUSIPCO)*. IEEE, 2018, pp. 647–651.

[12] S. Sreehari, S. Venkatakrishnan, B. Wohlberg, G. Buzzard, L. Drummy, J. Simmons, and C. Bouman, "Plug-and-play priors for bright field electron tomography and sparse interpolation," *IEEE Trans. Comput. Imaging*, vol. 2, no. 4, pp. 408–423, 2016.

[13] A. Teodoro, J. Bioucas-Dias, and M. Figueiredo, "A convergent image fusion algorithm using scene-adapted gaussian-mixture-based denoising," *IEEE Trans. Image Process.*, vol. 28, no. 1, pp. 451–463, 2018.

[14] X. Wang, J. Chen, C. Richard, and D. Brie, "Learning spectral-spatial prior via 3DDnCNN for hyperspectral image deconvolution," in *Proc. IEEE Int. Conf. Acoust., Speech, Signal Process. (ICASSP)*, 2020, pp. 2403–2407.

[15] S. Boyd, N. Parikh, E. Chu, B. Peleato, J. Eckstein, et al., "Distributed optimization and statistical learning via the alternating direction method of multipliers," *Found. Trends Mach. Learn.*, vol. 3, no. 1, pp. 1–122, 2011.

[16] A. Buades, B. Coll, and J.-M. Morel, "A non-local algorithm for image denoising," in *Proc. of IEEE Computer Society Conference on Computer Vision and Pattern Recognition (CVPR)*, 2005, vol. 2, pp. 60–65.

[17] K. Dabov, A. Foi, V. Katkovnik, and K. Egiazarian, "Image denoising by sparse 3-d transform-domain collaborative filtering," *IEEE Trans. Image Process.*, vol. 16, no. 8, pp. 2080–2095, 2007.

[18] M. Maggioni, V. Katkovnik, K. Egiazarian, and A. Foi, "Nonlocal transform-domain filter for volumetric data denoising and reconstruction," *IEEE Trans. Image Process.*, vol. 22, no. 1, pp. 119–133, 2012.

[19] J. Silván-Cárdenas and L. Wang, "Fully constrained linear spectral unmixing: Analytic solution using fuzzy sets," *IEEE Trans. Geosci. Remote Sens.*, vol. 48, no. 11, pp. 3992–4002, 2010.

[20] J. Bioucas-Dias and M. Figueiredo, "Alternating direction algorithms for constrained sparse regression: Application to hyperspectral unmixing," in *Proc. of Workshop on Hyperspectral Image and Signal Processing: Evolution in Remote Sensing*, 2010, pp. 1–4.

[21] Z. Shi, T. Shi, M. Zhou, and X. Xu, "Collaborative sparse hyperspectral unmixing using l_0 norm," *IEEE Trans. Geosci. Remote Sens.*, vol. 56, no. 9, pp. 5495–5508, 2018.

[22] J. M. Nascimento and J. M. Dias, "Vertex component analysis: A fast algorithm to unmix hyperspectral data," *IEEE Trans. Geosci. Remote Sens.*, vol. 43, no. 4, pp. 898–910, 2005.